Journal of Sound and Vibration (2001) **246**(3), 419–439
doi:10.1006/jsvi.2001.3637, available online at http://www.idealibrary.com on IDEAL®

DISCRETE HUYGENS' MODELLING SIMULATION OF SOUND WAVE PROPAGATION IN VELOCITY VARYING ENVIRONMENTS

Y. KAGAWA AND T. TSUCHIYA

Department of Electronics and Information Systems, Akita Prefectural University, Honjo, Akita 015-0055, *Japan. E-mail: Y.Kagawa@akita-pu-ac.jp*

T. HARA

Sharp Co. Ltd., tenri, Nara, 545-8522, *Japan*

AND

T. TSUJI

Kyocera-Mita Co. Ltd., Osaka, 540-8585, *Japan*

(*Received* 3 *July* 2000, *and in final form* 2 *January* 2001)

The discrete Huygens' modelling is used to simulate the process of the Huygens' principle in a discrete sense. The method and the modelling were proposed with the demonstration of possible fields of applications. In the present paper, an extension is made to the acoustic problems in which the propagation velocity varies depending on the environment. The two cases are considered, one is the case when the propagation velocity is dependent on the location but independent of the propagation direction. This case is demonstrated for the sound propagation in the ocean. Another is the case when the propagation speed depends on the direction of the propagation. This case is demonstrated for sound propagation in the medium with mean flow.

1. INTRODUCTION

The discrete Huygens' modelling is a realization of the Huygens' principle in a discrete sense in which the sequence of the impulse scattering is traced for each minimum distance of travel. The field is modelled here by Cartesian grid meshes made of acoustic tubes crossed at the connecting nodes in which the scattering occurs. The scattering takes place due to the impedance discontinuity at the nodes. Alternatively, the field is analogously replaced by grid meshes made of an electrical transmission-line network. The analogy approach has long been favored by electro-acoustic engineers for which both lumped and distributed parameter systems have been developed. The transmission-line modelling (TLM) approach was first developed by Johns [1] for electromagnetic field analysis, whose ingenuity is to provide the time domain solution as the results of the impulse responses. We applied the technique to acoustical systems but without much success due to the lack of computer capability at that time [2]. Recently, we have developed the approach for the acoustic problems, which are described in its own terminology without much referring to the electrical equivalence [3, 4]. This is the reason why we called the approach the discrete Huygens' modelling. In the present paper, we confine ourselves to the acoustic field in two dimension. We discuss two cases. One is the situation in which the propagation velocity is

0022-460X/01/380419 + 21 $35.00/0

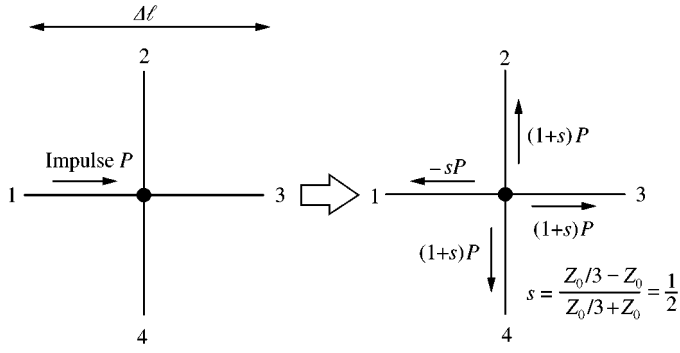

Figure 1. Impulse scattering at the element node.

independent of the propagation direction but dependent on the location. For this modelling, the element with five arms is used, in which the fifth arm is used for varying the propagation velocity. The example demonstrates the sound wave propagation in the ocean. Another is the situation in which the velocity depends on the direction of the propagation. This is modelled by providing a directionally coupled by-pass transmission line that bridges the fifth arms of two adjacent elements. The example demonstrates the sound wave propagation in a medium with mean flow.

2. VARIABLE PROPAGATION VELOCITY

2.1. THE CASE WHEN THE PROPAGATION VELOCITY IS INDEPENDENT OF DIRECTION

A two-dimensional minute wave field can be described by a square element (TLM, transmission-line matrix, line length $\Delta\ell$) consisting of four acoustic tubes connected at the center as shown in Figure 1. Each tube or branch has the characteristic impedance $Z_0 = \rho c_0$, where ρ is the medium density and c_0 is the propagation velocity in the medium. The transmission branches connected at the node create a network, which is nothing but a low-pass wave filter. The particular feature of the approach is that the sequences of impulses are traced in time domain. In the element, an input impulse P arriving at branch 1 is scattered at the node to reflect back to the same branch and to transmit toward other three branches. This is due to the impedance discontinuity at the connecting node. The impedance from one branch to the other three branches at the node is $Z_0/3$. This means that the impulse of strength $-P/2$ is reflected back to branch 1 and the impulses of strength $P/2$ are scattered to other branches. The scattered impulses then become the input impulses, respectively, to adjacent square elements. This process is repeated to create the propagation, which is what Huygens explained as the mechanism of the propagation of light. These impulses advance by the distance $\Delta\ell\ (= c_T \Delta t)$ for the time step Δt, where c_T is the propagation velocity of the wave over the network, that is $c_T = c_0/\sqrt{2}$, where c_0 is the propagation velocity in the free medium [3]. This algorithm is easily implemented on a computer.

The propagation velocity may be decreased by the introduction of a certain amount of volume at the node. This can equivalently be made by the introduction of the fifth branch of length $\Delta\ell/2$ with a proper characteristic impedance $Z_5 = Z_0/\eta$ closed at the other end, which are shown in Figure 2. The variable propagation velocity is now given by

$$c_T = \sqrt{\frac{2}{\eta + 4}}\, c_0. \tag{1}$$

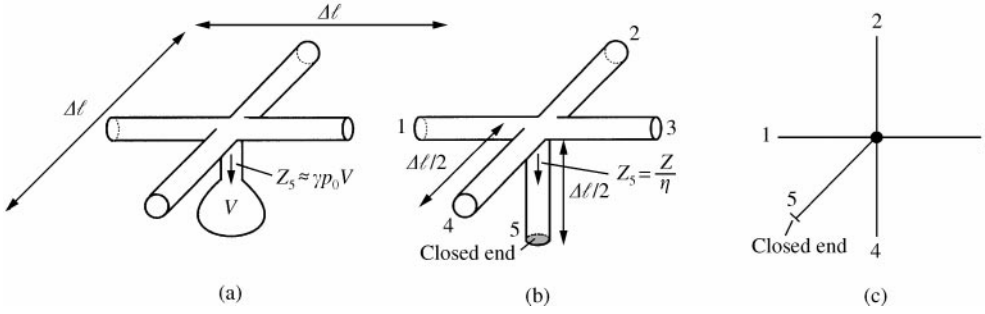

Figure 2. Element for propagation velocity variation; (a) lumped volume model γ: specific heat ratio $p_0 \approx p$: ambient pressure V: volume; (b) equivalent closed tube model for the fifth arm (velocity is controlled by the choice of parameter η); (c) transmission-line expression.

The velocity varies depending on parameter η chosen, which is the admittance of that branch measured in terms of Z_0. This treatment makes not to violate the synchronization of the impulses. This modelling has already been discussed in our previous paper [3].

2.2. THE CASE WHEN THE PROPAGATION VELOCITY IS DEPENDENT ON DIRECTION

2.1.1. *One-dimensional case with variable propagation velocity*

In the medium with flow, the speed of the sound wave propagation is directional. The speed of the sound propagation going down along the flow will be the sum of the propagation speed in the still medium and the speed of the flow, while the propagation speed of the sound going up against the flow will be the propagation speed in the still medium minus the flow speed. First, we consider the case without flow. The one-dimensional sound field is described by the sound waves in an acoustic tube. The discrete Huygens' model uses a series of the acoustic tube segments of length $\Delta\ell$ with a node at its center as shown in Figure 3, in which impulses pass through the node without scattering. The relations of the velocity potential ${}_k\phi_i$ at the node i at time $t = k\Delta t$ $(k = 0, 1, 2, \ldots)$ to the input impulses ${}_k\phi_i^n$ and the output (transmitted, reflected) impulses ${}_{k+1}\psi_i^n$ are given by

$$ {}_k\phi_i = \sum_{m=1}^{2} {}_k\phi_i^m, $$

$$ {}_{k+1}\psi_i^n = {}_k\phi_i - {}_k\phi_i^n \quad (n = 1, 2), \tag{2} $$

where superscript n refers to the branch number. The scattering matrix expression of equation (2) is given by

$$ {}_{k+1}\begin{bmatrix} \psi_i^1 \\ \psi_i^2 \end{bmatrix} = \begin{bmatrix} 0 & 1 \\ 1 & 0 \end{bmatrix}_k \begin{bmatrix} \phi_i^1 \\ \phi_i^2 \end{bmatrix}. \tag{3} $$

It takes time Δt for the impulse to transmit length $\Delta\ell$. The subscript k refers to the number of the time step. The relation of the input impulse to the output impulse, or the continuity

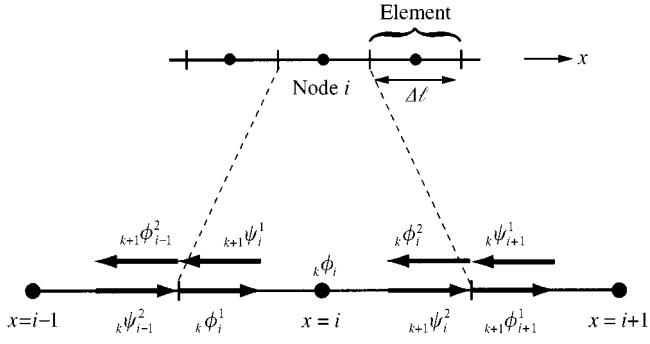

Figure 3. One-dimensional field model.

condition is

$$ {}_k\phi^1_{i+1} = {}_k\psi^2_i, \qquad {}_k\phi^2_{i-1} = {}_k\psi^1_i. \tag{4} $$

From equations (2) and (4), one obtains the expression

$$ {}_{k+1}\phi_i - 2{}_k\phi_i + {}_{k-1}\phi_i = {}_k\phi_{i+1} - 2{}_k\phi_i + {}_k\phi_{i-1}. \tag{5} $$

This is the finite difference-time domain expression, which can be expanded in Taylor series about ${}_k\phi_i$ to give the differential expression

$$ \frac{\partial^2\phi}{\partial t^2} - c^2\frac{\partial^2\phi}{\partial x^2} + 2\left\{\frac{\Delta t^2}{4!}\left(\frac{\partial^4\phi}{\partial t^4} - c^4\frac{\partial^4\phi}{\partial x^4}\right) + \frac{\Delta t^4}{6!}\left(\frac{\partial^6\phi}{\partial t^6} - c^6\frac{\partial^6\phi}{\partial x^6}\right) + \cdots\right\} = 0, \tag{6} $$

where the subscripts k and i are ignored as the point of the interest can be taken anywhere in the ordinate, and c is the transmission speed of the impulse over the network, which is defined by

$$ c = \Delta\ell/\Delta t = c_0. \tag{7} $$

This propagation velocity is the same as in free space. Equation (6) corresponds to the wave equation for ϕ with some higher order error terms

$$ \frac{\partial^2\phi}{\partial t^2} - c^2\frac{\partial^2\phi}{\partial x^2} + \text{error terms} = 0. \tag{8} $$

The error term is of the order of $O(\Delta t^2)$.

The variable speed of propagation can be achieved by providing the third branch with the characteristic impedance $Z_3 = Z_0/\eta$, which is illustrated in Figure 4. For the case of the variable sound speed, similar relations to equation (2) are given by

$$ {}_k\phi_i = \frac{2}{\eta+2}\sum_{m=1}^{2} {}_k\phi^m_i + \frac{2\eta}{\eta+2}{}_k\phi^3_i, $$

$$ {}_{k+1}\psi^n_i = {}_k\phi_i - {}_k\phi^n_i \quad (n = 1, 2, 3). \tag{9} $$

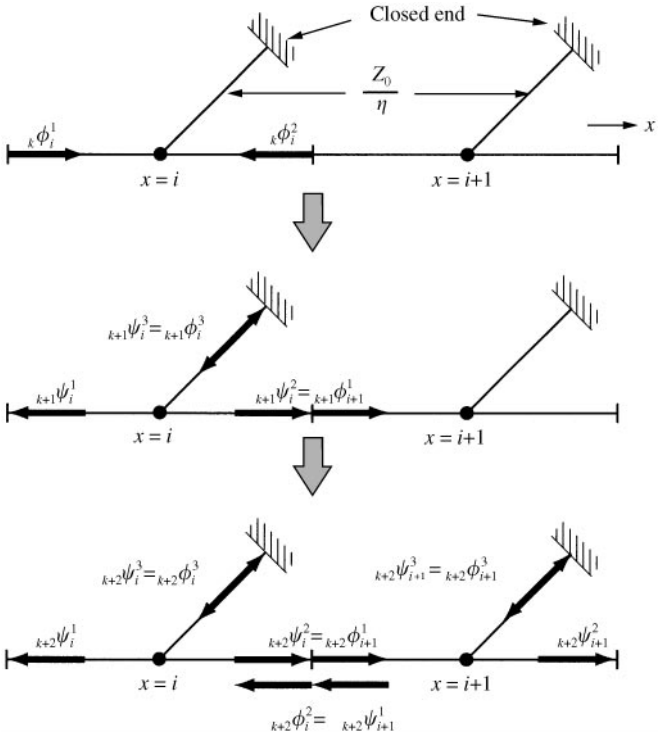

Figure 4. Impulse transmission and scattering.

The scattering matrix expression is

$$_{k+1}\begin{bmatrix}\psi_i^1\\ \psi_i^2\\ \psi_i^3\end{bmatrix} = \frac{1}{\eta+2}\begin{bmatrix}-\eta & 2 & 2\eta\\ 2 & -\eta & 2\eta\\ 2 & 2 & \eta-2\end{bmatrix}_k\begin{bmatrix}\phi_i^1\\ \phi_i^2\\ \phi_i^3\end{bmatrix}. \tag{10}$$

The condition of continuity is given by

$$_k\phi_{i+1}^1 = {}_k\psi_i^2, \qquad {}_k\phi_{i-1}^2 = {}_k\psi_i^1, \qquad {}_k\phi_i^3 = {}_k\psi_i^3. \tag{11}$$

From equations (9) and (11), the finite difference expression similar to equation (5) is obtained as

$$_{k+1}\phi_i - 2_k\phi_i + {}_{k-1}\phi_i = \frac{2}{\eta+2}({}_k\phi_{i+1} - 2_k\phi_i + {}_k\phi_{i-1}). \tag{12}$$

The wave equation can then be found to be

$$\frac{\partial^2\phi}{\partial t^2} - \frac{2}{\eta+2}c^2\frac{\partial^2\phi}{\partial x^2} + 2\left\{\frac{\Delta t^2}{4!}\left(\frac{\partial^4\phi}{\partial t^4} - \frac{2}{\eta+2}c^4\frac{\partial^4\phi}{\partial x^4}\right) + \frac{\Delta t^4}{6!}\left(\frac{\partial^6\phi}{\partial t^6} - \frac{2}{\eta+2}c^6\frac{\partial^6\phi}{\partial x^6}\right) + \cdots\right\} = 0. \tag{13}$$

Equation (13) also indicates the wave equation

$$\frac{\partial^2\phi}{\partial t^2} - \frac{2}{\eta+2}\,c^2\,\frac{\partial^2\phi}{\partial x^2} + \text{error terms} = 0. \tag{14}$$

The propagation speed is thus given as

$$c_T = \sqrt{\frac{2}{\eta+2}}\,c. \tag{15}$$

The propagation speed depends on the parameter η ($c_T \leqslant c$) [3, 4].

2.2.2. *Modelling in the medium with mean flow*

The wave equation governing the wave propagation in the medium with mean flow is known to be [5]

$$\frac{\partial^2\phi}{\partial t^2} + 2v\,\frac{\partial^2\phi}{\partial t\,\partial x} - (c_0^2 - v^2)\,\frac{\partial^2\phi}{\partial x^2} = 0, \tag{16}$$

where c_0 is the propagation speed when there is no flow, and v is the speed of the flow in the x direction. The particle velocity $\mathbf{u}$, and the sound pressure p are defined as

$$\mathbf{u} = -\nabla\phi, \tag{17}$$

$$p = \rho\left(\frac{\partial\phi}{\partial t} + v\,\frac{\partial\phi}{\partial x}\right). \tag{18}$$

Here, we consider a model in which impulses scatter from the node into the third branch which transmit into the third branch of the adjacent element in the downstream without delay as shown in Figure 5. The scattering expressions for this case are the same as equations (9) and (10), except for the condition of continuity. For the third branch, it is different from equation (11), which is

$${}_k\phi^3_{i+1} = {}_k\psi^3_i. \tag{19}$$

It should be noted that in the third branches, the scattering and transmission are uni-directional. From equations (9) and (19), in a similar manner as in the previous case, the finite difference expression results in

$$\begin{aligned}
&({}_{k+1}\phi_i - 2{}_k\phi_i + {}_{k-1}\phi_i) + ({}_k\phi_{i-1} - 2{}_{k-1}\phi_{i-1} + {}_{k-2}\phi_{i-1})\\
&= \frac{2}{\eta+2}\{({}_k\phi_{i+1} - 2{}_k\phi_i + {}_k\phi_{i-1}) + ({}_{k-1}\phi_i - 2{}_{k-1}\phi_{i-1} + {}_{k-1}\phi_{i-2})\}\\
&\quad - \frac{2\eta}{\eta+2}\{({}_k\phi_i - {}_k\phi_{i-1}) - ({}_{k-1}\phi_i - {}_{k-1}\phi_{i-1})\}.
\end{aligned} \tag{20}$$

The finite difference expression expanded in Taylor series lead to the differential expression

$$\begin{aligned}
&\frac{\partial^2\phi}{\partial t^2} + \frac{\eta}{\eta+2}\,c\,\frac{\partial^2\phi}{\partial t\,\partial x} - \frac{2}{\eta+2}\,c^2\,\frac{\partial^2\phi}{\partial x^2}\\
&+ \left\{\frac{1}{2!}\left(\frac{\partial^2}{\partial t^2} - \frac{\eta}{\eta+2}\,c^2\,\frac{\partial^2}{\partial x^2}\right) + \frac{\Delta t^2}{4!}\left(\frac{\partial^4}{\partial t^4} - \frac{\eta}{\eta+2}\,c^4\,\frac{\partial^4}{\partial x^4}\right) + \cdots\right\}
\end{aligned}$$

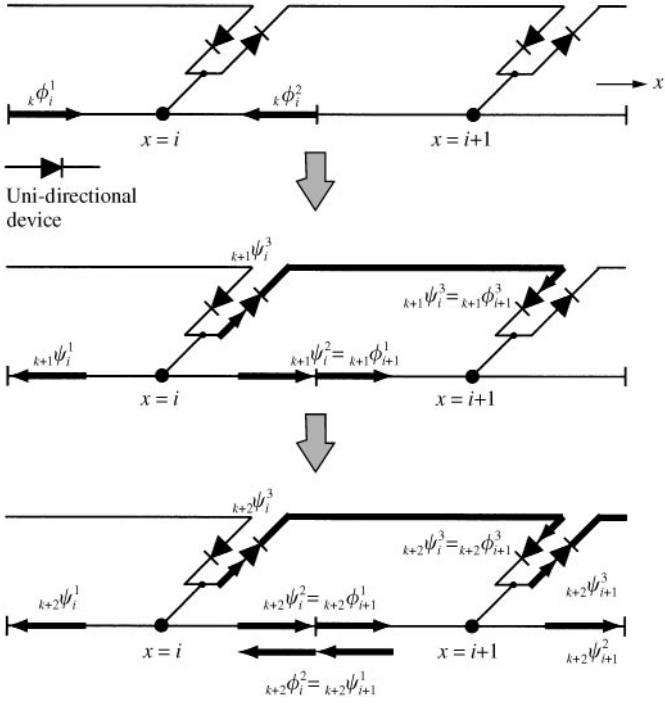

Figure 5. Directional link of scattered impulses to the adjacent branch.

$$\times\left\{\Delta t\left(\frac{\partial\phi}{\partial t}-c^2\frac{\partial\phi}{\partial x}\right)+\frac{\Delta t^2}{2!}\left(\frac{\partial^2\phi}{\partial t^2}+c^2\frac{\partial^2\phi}{\partial x^2}\right)+\frac{\Delta t^3}{3!}\left(\frac{\partial^3\phi}{\partial t^3}-c^3\frac{\partial^3\phi}{\partial x^3}\right)+\cdots\right\}$$

$$+2\left\{\frac{\Delta t^2}{4!}\left(\frac{\partial^4\phi}{\partial t^4}-\frac{\eta}{\eta+2}c^4\frac{\partial^4\phi}{\partial x^4}\right)+\frac{\Delta t^4}{6!}\left(\frac{\partial^6\phi}{\partial t^6}-\frac{\eta}{\eta+2}c^6\frac{\partial^6\phi}{\partial x^6}\right)+\cdots\right\}$$

$$-\frac{\eta}{\eta+2}c^2\left(\frac{1}{2!}\frac{\partial^2}{\partial x^2}-\frac{\Delta\ell}{3!}\frac{\partial^3}{\partial x^3}+\frac{\Delta\ell^2}{4!}\frac{\partial^4}{\partial x^4}-\cdots\right)\left(\Delta t\frac{\partial\phi}{\partial t}+\frac{\Delta t^2}{2!}\frac{\partial^2\phi}{\partial t^2}+\cdots\right)$$

$$+\frac{\eta}{\eta+2}c\frac{\partial}{\partial x}\left(\frac{\Delta t}{2!}\frac{\partial^2\phi}{\partial t^2}+\frac{\Delta t^2}{3!}\frac{\partial^3\phi}{\partial t^3}+\cdots\right)=0. \tag{21}$$

Therefore,

$$\frac{\partial^2\phi}{\partial t^2}+\frac{\eta}{\eta+2}c\frac{\partial^2\phi}{\partial t\,\partial x}-\frac{2}{\eta+2}c^2\frac{\partial^2\phi}{\partial x^2}+\text{ error terms}=0. \tag{22}$$

Comparing with equation (16) gives the relation

$$c=\frac{\eta+4}{2\eta+4}c_0,\qquad v=\frac{\eta}{2\eta+4}c_0, \tag{23, 24}$$

where c_0 is the propagation speed without the medium flow, and v is the velocity of the medium flow. The propagation velocity and flow velocity are depending on the choice of η,

which cannot independently be adjusted. Equation (22) only requires that the correspondence between the propagation speed in the space and that in the network should always be coincident.

2.2.3. *Two-dimensional case with mean flow*

The extension to the two-dimensional field problems is straightforward. The wave equation is given by

$$\frac{\partial^2\phi}{\partial t^2} + 2v\frac{\partial^2\phi}{\partial t\,\partial x} - (c_0^2 - v^2)\frac{\partial^2\phi}{\partial x^2} - c_0^2\frac{\partial^2\phi}{\partial y^2} = 0 \tag{25}$$

in which the mean flow is only directed along the x-axis. For the propagation speed variation, the fifth branch is added to a two-dimensional element with four branches. The fifth branches are now coupled between two adjacent elements in the same way as in the one-dimensional modelling. The modelling is shown in Figure 6, in which the relation of the impulses is

$$\begin{aligned} {}_k\phi_{i,j} &= \frac{2}{\eta+4}\sum_{m=1}^{4} {}_k\phi_{i,j}^m + \frac{2\eta}{\eta+4}\,{}_k\phi_{i,j}^5, \\ {}_k\psi_{i,j}^n &= {}_k\phi_{i,j} - {}_k\phi_{i,j}^n \quad (n = 1\text{–}5). \end{aligned} \tag{26}$$

The scattering matrix expression is given by

$$\begin{bmatrix} \psi_{i,j}^1 \\ \psi_{i,j}^2 \\ \psi_{i,j}^3 \\ \psi_{i,j}^4 \\ \psi_{i,j}^5 \end{bmatrix}_{k+1} = \frac{2}{\eta+4}\begin{bmatrix} -1-\eta/2 & 1 & 1 & 1 & \eta \\ 1 & -1-\eta/2 & 1 & 1 & \eta \\ 1 & 1 & -1-\eta/2 & 1 & \eta \\ 1 & 1 & 1 & -1-\eta/2 & \eta \\ 1 & 1 & 1 & 1 & -2+\eta/2 \end{bmatrix}\begin{bmatrix} \phi_{i,j}^1 \\ \phi_{i,j}^2 \\ \phi_{i,j}^3 \\ \phi_{i,j}^4 \\ \phi_{i,j}^5 \end{bmatrix}_k. \tag{27}$$

The condition of continuity is given by

$$\begin{aligned} &{}_k\phi_{i+1,j}^1 = {}_k\psi_{i,j}^3, \qquad {}_k\phi_{i,j-1}^2 = {}_k\psi_{i,j}^4, \qquad {}_k\phi_{i-1,j}^3 = {}_k\psi_{i,j}^1, \\ &{}_k\phi_{i,j+1}^4 = {}_k\psi_{i,j}^2, \qquad {}_k\phi_{i+1,j}^5 = {}_k\psi_{i,j}^5. \end{aligned} \tag{28}$$

From them it is easy to obtain the finite difference expression as follows:

$$\begin{aligned} &({}_{k+1}\phi_{i,j} - 2{}_k\phi_{i,j} + {}_{k-1}\phi_{i,j}) + ({}_k\phi_{i-1,j} - 2{}_{k-1}\phi_{i-1,j} + {}_{k-2}\phi_{i-1,j}) \\ &= \frac{2}{\eta+4}\{({}_k\phi_{i+1,j} - 2{}_k\phi_{i,j} + {}_k\phi_{i-1,j}) + ({}_{k-1}\phi_{i,j} - 2{}_{k-1}\phi_{i-1,j} + {}_{k-1}\phi_{i-2,j}) \\ &\quad + ({}_k\phi_{i,j+1} - 2{}_k\phi_{i,j} + {}_k\phi_{i,j-1}) + ({}_{k-1}\phi_{i-1,j+1} - 2{}_{k-1}\phi_{i-1,j} + {}_{k-1}\phi_{i-1,j-1})\} \\ &\quad - \frac{2\eta}{\eta+4}\{({}_k\phi_{i,j-k}\phi_{i-1,j}) - ({}_{k-1}\phi_{i,j} - {}_{k-1}\phi_{i-1,j})\}. \end{aligned} \tag{29}$$

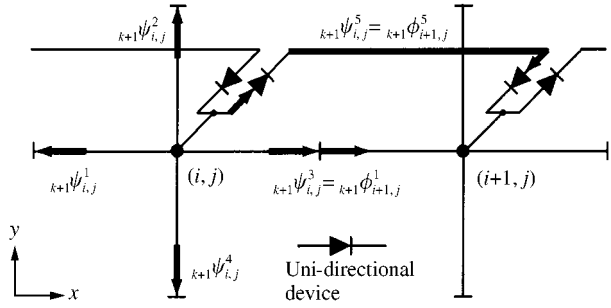

Figure 6. Impulse scattering and transmission in two adjacent elements in two dimension.

The finite difference expression again leads to the differential equation with some error terms

$$\frac{\partial^2\phi}{\partial t^2} + \frac{\eta}{\eta+4}\,c\,\frac{\partial^2\phi}{\partial t\,\partial x} - \frac{2}{\eta+4}\,c^2\,\frac{\partial^2\phi}{\partial x^2} - c\,\frac{\partial^2\phi}{\partial y^2} + \text{error terms} = 0. \tag{30}$$

Comparing with equation (25) gives the relation

$$c = \frac{\sqrt{(\eta+4)^2+16}}{2\eta+8}\,c_0, \qquad v = \frac{\eta}{2\eta+8}\,c_0. \tag{31, 32}$$

3. DEMONSTRATIONS

3.1. THE SOUND PROPAGATION IN THE OCEAN

The distribution of the sound speed in the ocean is depicted in Figure 7, in which some distinctive modes of propagation are also illustrated [6]. The direction of the sound wave propagation is likely to bend in the place where the sound speed has gradient. Some distinctive sound propagation modes include surface channel propagation, SOFAR channel propagation, bottom bounce propagation and convergence zone propagation. They sometimes form a shadow zone. The surface channel propagation is the mode in which sound wave repeats the multiple reflections just below the surface. This channel is the sea surface layer of some hundred meters in depth where the temperature is constant under the surface before it goes down. In this region, sound wave is trapped within the channel as sound waves directed within a certain angle are propagating reflectively between the water surface and the bottom of the channel. The waves other than these are likely to go down towards the bottom. A shadow zone is created, to which the sound waves less reach. The sound waves going down are reflected at the bottom in the sea bed (about 5000 m under the sea surface), which is the bottom bounce propagation or if the sea is very deep, waves go back upward before they reach the bottom. The latter waves refractively propagate between the sea surface and the sea bed, which is the convergence zone propagation. At the depth of about 1000 m, sound speed reaches the minimum, which creates a layer so-called SOund Fixing And Ranging (SOFAR) channel. If sound is emitted near the SOFAR channel, the sound waves are trapped repeating upward and downward refraction. This propagation mode is called SOFAR channel propagation. The purpose of the present paper is just to investigate how the present modelling could be applied to demonstrate the distinctive modes of propagation under such a temperature gradient environment.

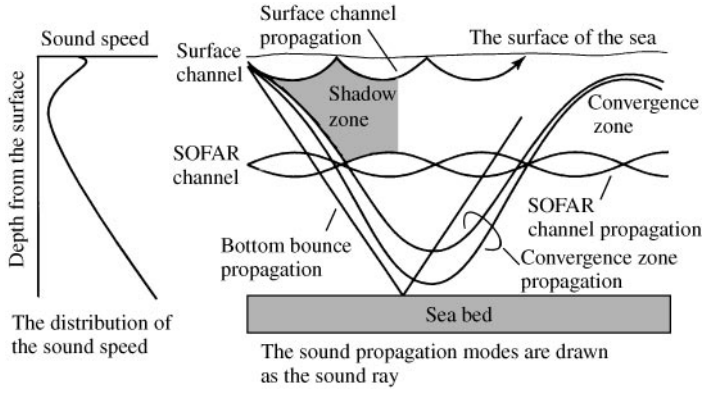

Figure 7. The modes of sound propagation in the ocean.

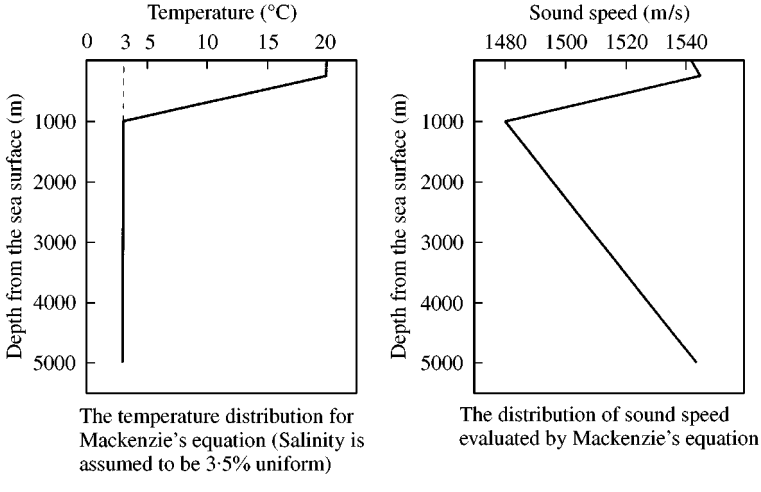

Figure 8. The distribution of temperature and sound speed assumed for the present simulation; (a) the temperature distribution for Mackenzie's equation (Salinity is assumed to be 3·5% uniform); (b) the distribution of sound speed evaluated by Mackenzie's equation.

3.1.1. *The relation between temperature and sound speed in the ocean*

In the ocean, sound speed not only depends on the temperature but also on the salinity and the water pressure. Mackenzie's nine-term equation for sound speed variation is employed here [7]. The sound speed c (m/s) is given by

$$c = 1448{\cdot}96 + 4{\cdot}591T - 5{\cdot}304 \times 10^{-2}T^2 + 2{\cdot}374 \times 10^{-4}T^3 + 1{\cdot}340(S - 35)$$
$$+ 1{\cdot}630 \times 10^{-2}D + 1{\cdot}675 \times 10^{-7}D^2 - 1{\cdot}025 \times 10^{-2}T(S - 35)$$
$$- 7{\cdot}139 \times 10^{-13}TD^3, \tag{33}$$

where T is the temperature (°C), S the salinity (%) and D the depth from the surface (m).

Figure 8 shows the temperature distribution and the corresponding sound speed evaluated by Mackenzie's equation, in which, positive gradient of sound speed in the surface

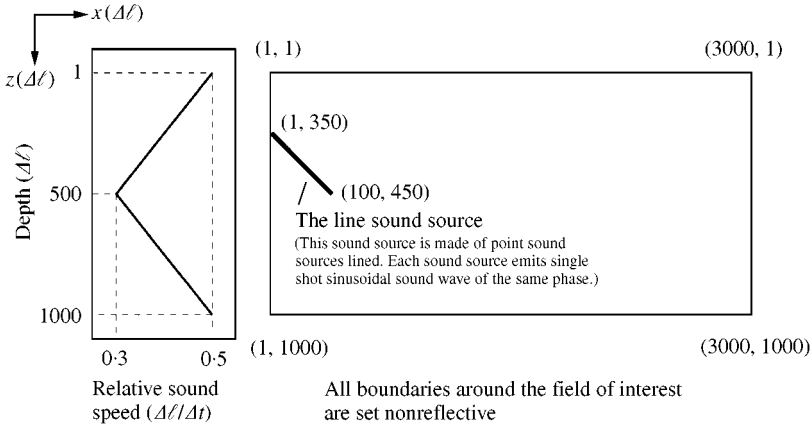

Figure 9. Two-dimensional model for simulating SOFAR channel propagation; (a) relative sound speed ($\Delta\ell/\Delta t$); (b) all boundaries around the field of interest are non-reflective.

channel and the presence of the minimum point of sound speed in SOFAR channel are shown.

3.1.2. *SOFAR channel propagation*

The SOFAR channel propagation is simulated first. This is the mode that appears at the depth of around 1000 m where sound speed reaches the minimum as shown in Figure 8. Although the simulation confines itself to the two-dimensional space, it is not easy to cover the whole range of interest, so that, as shown in Figure 9, only the region where the sound speed varies as the valley-like characteristic is considered. The sound speed is assumed to change linearly around the minimum point. A single shot sinusoidal wave consisting of the impulse train of 100 Δt with the amplitude of 200 dB (nonlinear effect not included, 0 dB is referred to 1 μPa) is used for excitation. A line sound source is assumed as shown in Figure 9 with a certain inclination. A non-reflective boundary condition is set for all the boundaries of the field of interest. When the sound speed is chosen to be 0·5 $\Delta\ell/\Delta t$, the wavelength corresponds to 50 $\Delta\ell$ and the source consists of 50 impulses. Figure 10 is the trace of the sound propagation at 10 000 Δt after the first sound emission from the source. The brightness of the spots depends on the sound intensity at the nodes of the elements. Sound is seen trapped within a channel between a certain width of 500 $\Delta\ell$ repeating upward and downward refraction around the line where the sound speed is minimum. Snell's law provides the ray trace of the shortest wavelength limit. The ray is also depicted in the figure for comparison. The sound source for Snell's law calculation is assumed to be perpendicular to the line source. It should be noted that the refraction is responsible for the change of the direction of sound propagation so that the direction of the sound going down again goes upward at a certain lower level. The present simulation includes the spill of the sound waves, in which some broader width of the sound waves is seen. It is, however, surprising that the classical Snell's law can provide a good estimate for the propagation path.

3.1.3. *Surface channel propagation*

The surface channel propagation is then investigated. Just under the surface, there exists the field where the positive gradient sound speed distribution turns into the negative gradient at around 300 $\Delta\ell$. The field to be modelled is shown with the sound source in

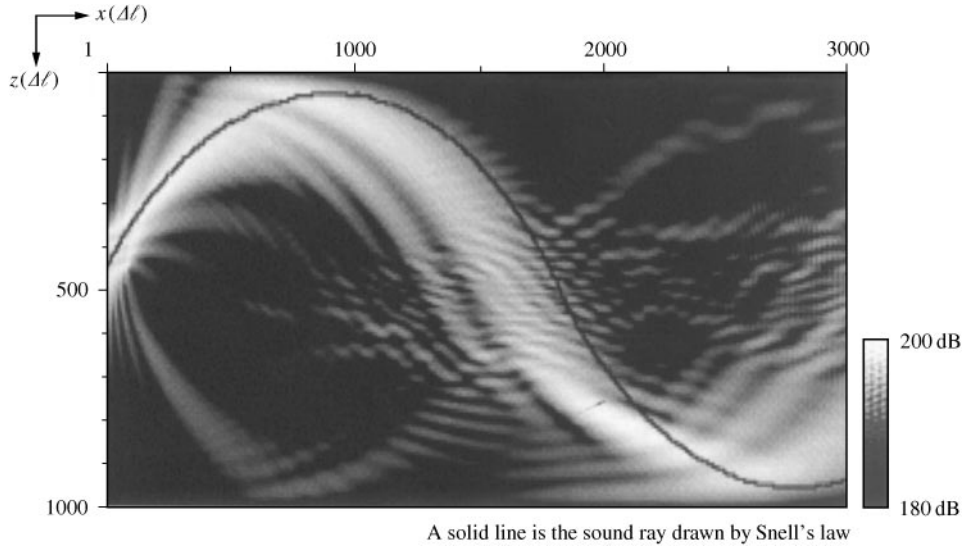

Figure 10. The trace of the sound propagation after 10^4 Δt from the first sound emission of 200 dB.

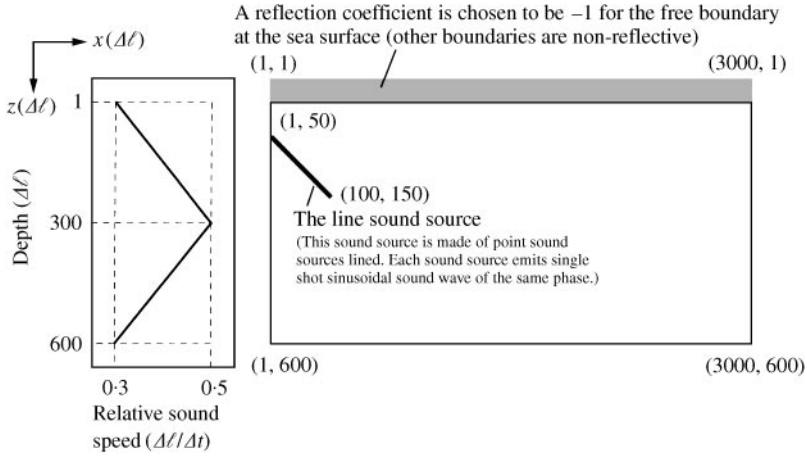

Figure 11. Two-dimensional model for simulating surface channel propagation.

Figure 11 in which the sound speed distribution is also given. For this case, the upper edge is the water surface, where the reflection coefficient is set to be -1 (at $z = 1$) for the free boundary. A sinusoidal wave consisting of the impulse train of 100 Δt is again used for the excitation of the line array. Figure 12 shows the trace of the sound propagation at 10 000 Δt after the sound emission. Sound waves propagate by repeating the reflection at the surface and refraction at a certain depth, to create the surface channel. Some waves spill out from the channel, which are going downward. There is a region to which sound waves less reach to form the shadow zone.

The sound rays are traced based on Snell's law, which are also depicted in the figure for comparison. Two point sound sources, as shown in Figure 13, are used for the ray traces. Snell's sound ray trace from the sound source ① follows the route of the simulated. Snell's sound ray trace from the sound source ② goes downward. From these results, we see that

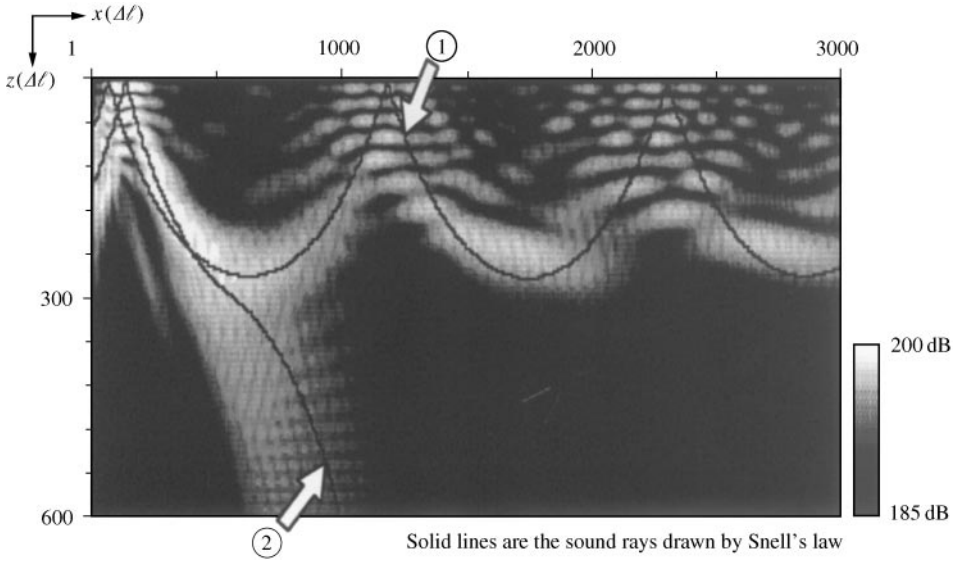

Figure 12. Simulated example for the surface channel propagation at 10^4 Δt, where the waves are partly split downward. Snell's sound rays are also shown for comparison.

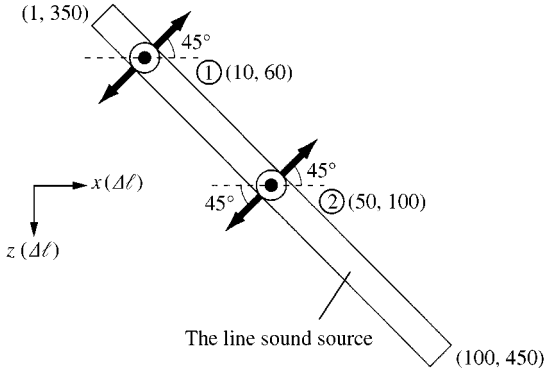

Figure 13. The line sound source and the point sources for the ray trace by Snell's law.

the route of the propagation or the mode of propagation depends on the location and direction of the sound source.

Snell's law is only valid in the limit of the shortest wavelength. So, the case of the sound source with shorter wavelength of 20 Δt is then considered. The result at 10 000 Δt is shown in Figure 14 together with Snell's sound rays, in which the silent regions are more pronounced.

3.1.4. *Convergence zone propagation*

Last of all, convergence zone propagation is considered for simulation. This mode of simulation requires a wider domain of field. The distribution of the sound speed and the location of the sound source are shown in Figure 15. A non-reflective boundary is again set except at the sea surface of free boundary. A single shot sinusoidal wave of 20 Δt is used for the excitation. Figure 16 shows the situation at 17 000 Δt. The sound ray due to Snell's

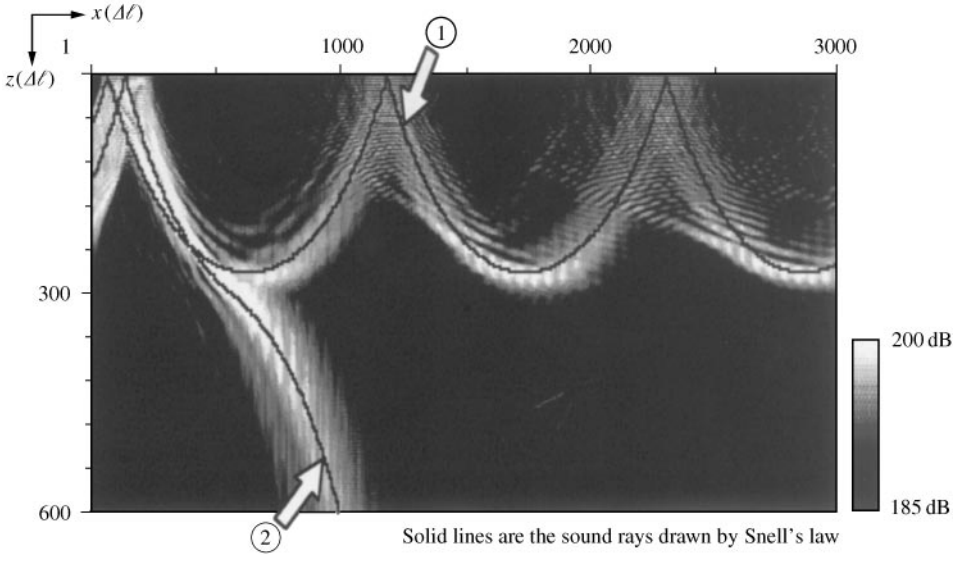

Figure 14. Same as the case of Figure 10 except for the sound source with shorter wavelength (20 Δt).

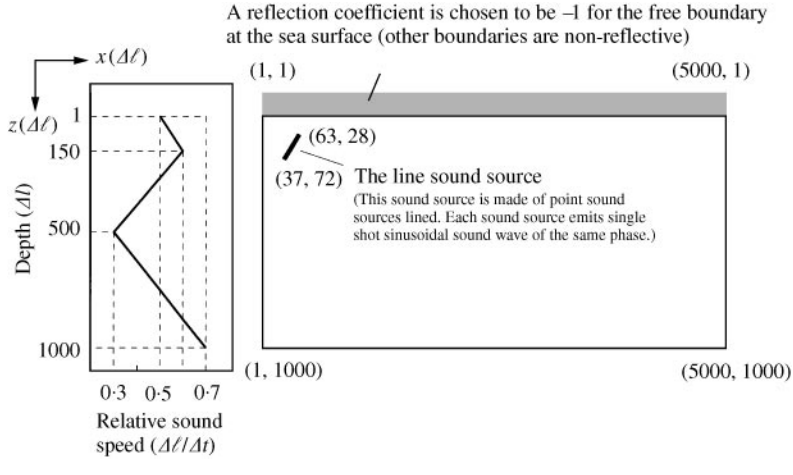

Figure 15. The condition of simulation for the convergence zone propagation.

formula is also depicted. The waves going downward are refracted back upward at around $z = 1000\ \Delta\ell$ before they reach the bottom. The waves converge near the surface at around $x = 2700\ \Delta\ell$, and are then reflected downward again. This is the convergence zone propagation. We see the waves that reach the bottom. Some waves also propagate trapped in the surface channel. For this excitation no wave is trapped in the SOFAR channel.

3.2. SOUND PROPAGATION IN MEAN FLOW FIELD

3.2.1. *One-dimensional field*

For the validity of the model developed in the previous section, a numerical examination is carried out. We consider the one-dimensional field as shown in Figure 17, in which the

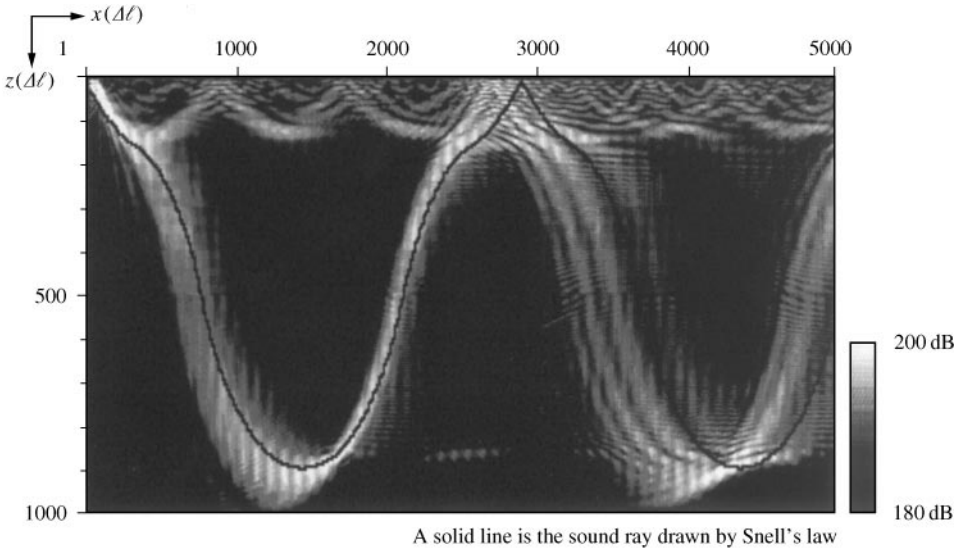

Figure 16. The traces of the wave propagation at $1{\cdot}7 \times 10^4\ \Delta t$, compared with Snell's sound rays.

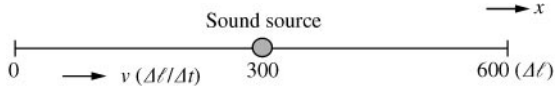

Figure 17. One-dimensional field with mean flow in which a source is placed at the center.

excitation is made at the midpoint of the field. The input is a single shot sine wave of the duration 100 Δt. Mach number $M(=v/c_0)$ of the flow is chosen to be 0·111 for $\eta = 0{\cdot}5$. This corresponds to the propagation speed $c = 0{\cdot}9c_0$ and flow velocity $v = 0{\cdot}1c_0$. The wave propagates toward both directions and the process of the wave propagation is shown in Figure 18.

3.2.2. *Finite difference solution*

Equation (16) can be solved directly by means of the finite difference scheme of

$$
{}_{k+1}\phi_i = 2{}_k\phi_i - {}_{k-1}\phi_i - 2v\frac{\Delta t}{\Delta \ell}\{({}_k\phi_i - {}_k\phi_{i-1}) - ({}_{k-1}\phi_i - {}_{k-1}\phi_{i-1})\}
$$

$$
- (v^2 - c_0^2)\left(\frac{\Delta t}{\Delta \ell}\right)^2 \{{}_k\phi_{i+1} - 2{}_k\phi_i + {}_k\phi_{i-1}\}. \tag{34}
$$

The same case as in the previous section is considered. Figure 19 shows the finite difference solution, in which the potential waveforms are distorted and the amplitudes of the particle velocity are depressed as the waves travel. When the meshes as fine as 10 times were used, the solution is as good as that of our present model. It is found that the present model thus provides a much better solution than that of the finite difference counterpart for the same discretization. The examination is extended to various Mach numbers or η. The errors of the travelled distance for the time required, evaluated at the peak of the wave are shown in Figure 20. The agreement is reasonable supporting the validity of the modelling.

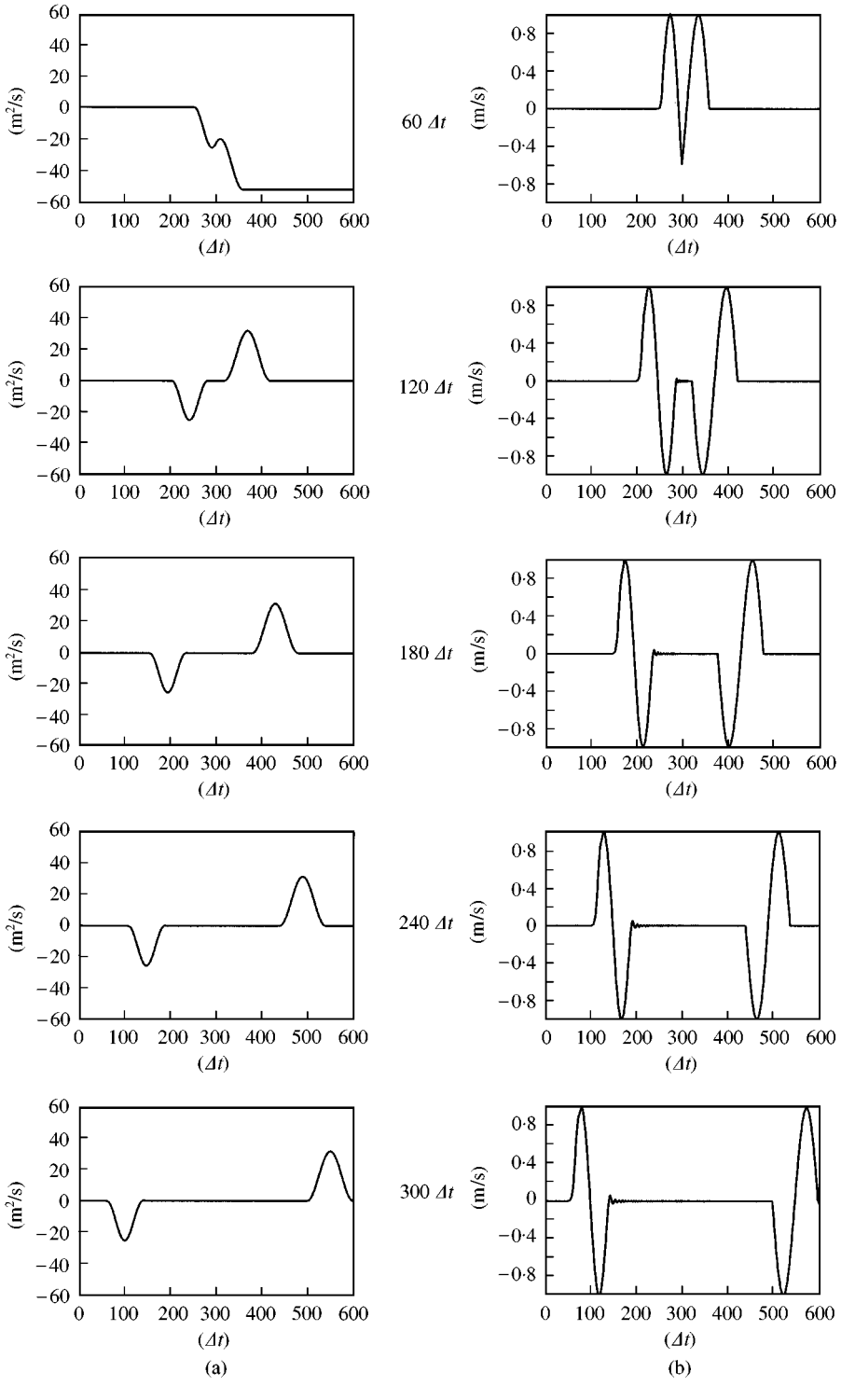

Figure 18. Wave propagation ($c = 0{\cdot}9c_0$, $v = 0{\cdot}1c_0$); (a) velocity potential ϕ; (b) particle velocity u.

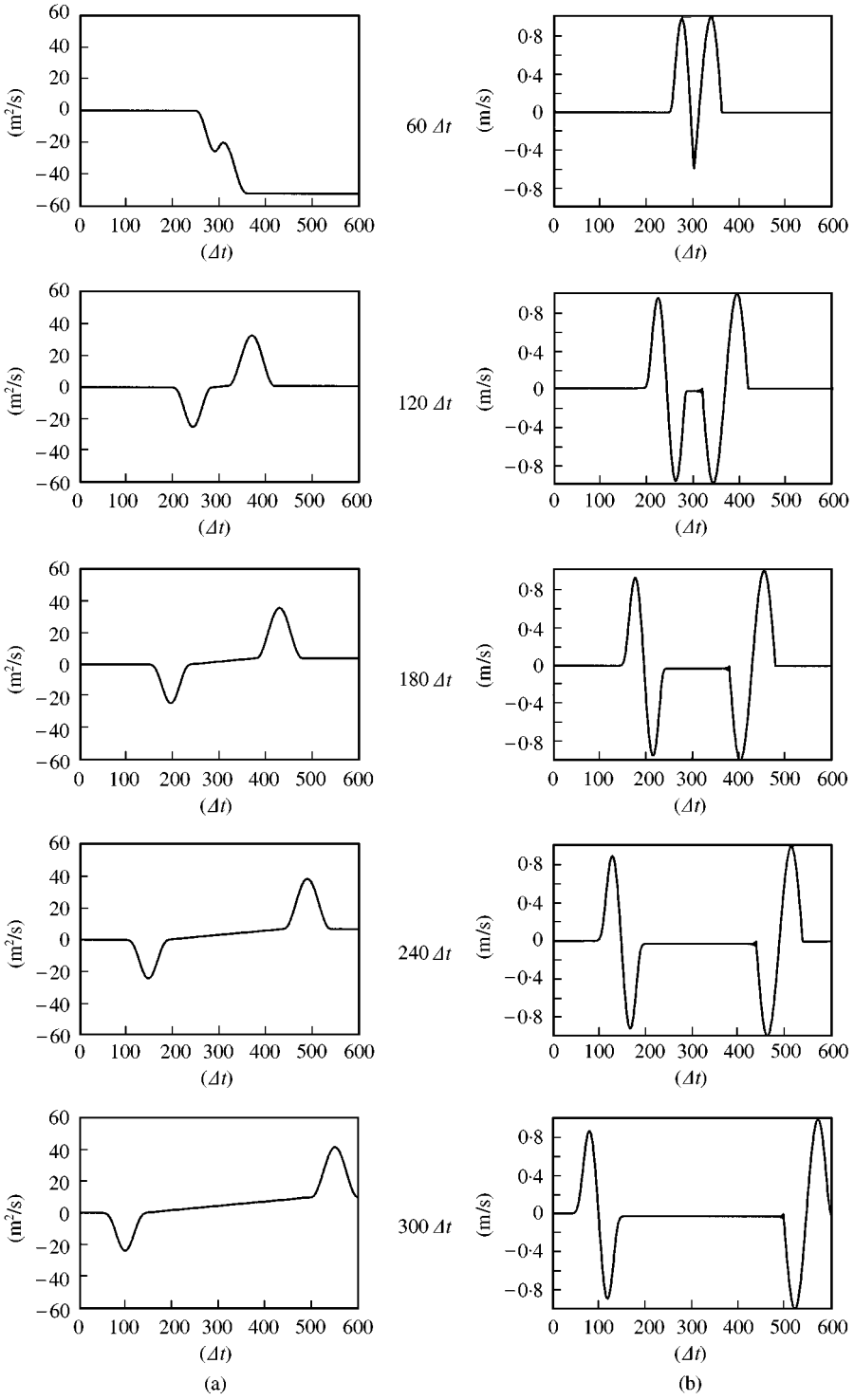

Figure 19. Wave propagation (FD-TD scheme: $c = 0{\cdot}9c_0, v = 0{\cdot}1c_0$); (a) velocity potential ϕ; (b) particle velocity u.

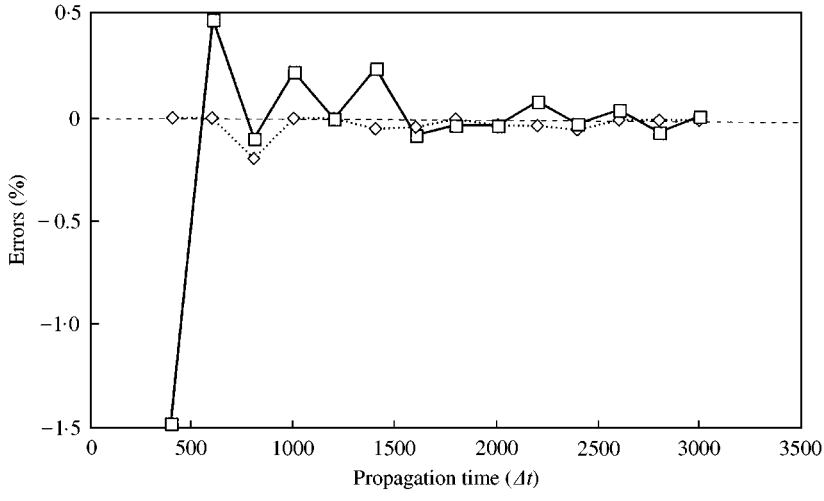

Figure 20. Errors in propagation speed; —□— Huygens' model, ·····◇····· finite difference (meshes as fine as 10 times are used).

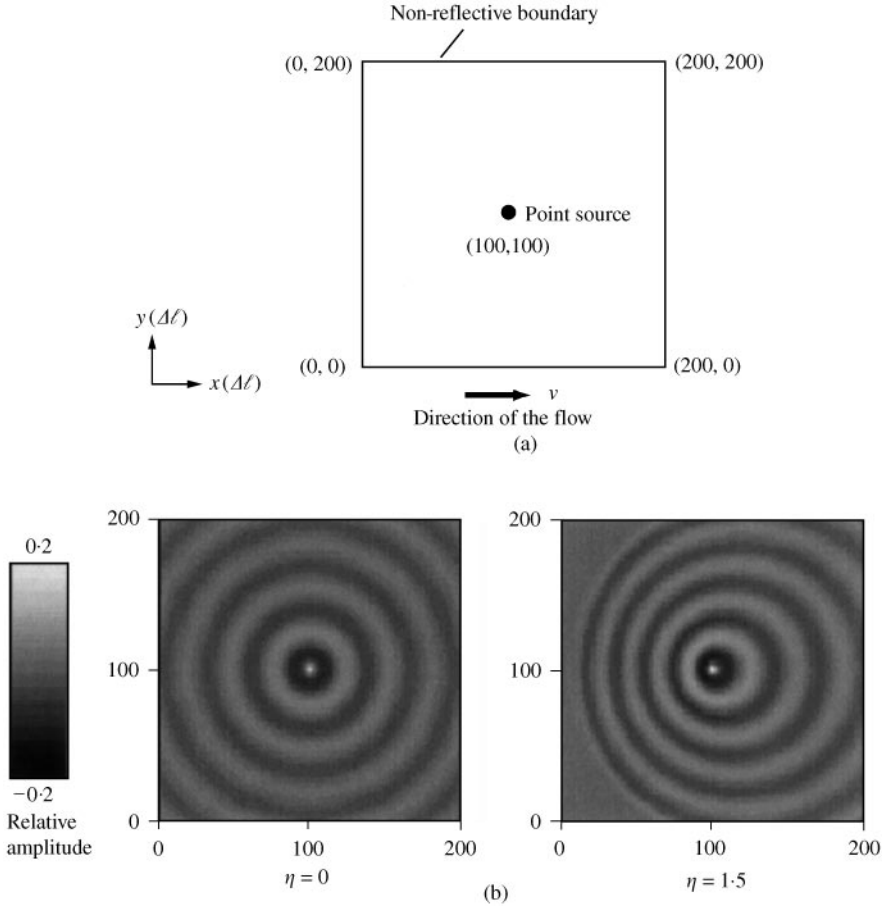

Figure 21. Wave propagation under mean flow; (a) field model, one shot sine wave of the duration 40 Δt, $\eta = 1{\cdot}5$, (b) distribution (after 200 Δt).

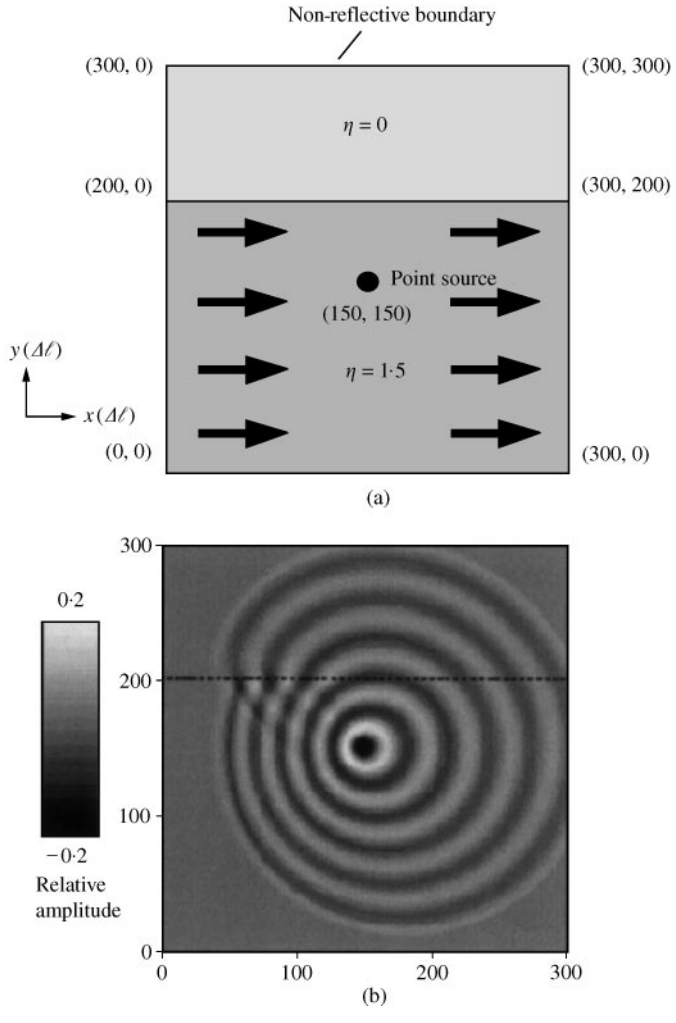

Figure 22. Wave propagation under partial mean flow; (a) field model; (b) distribution.

3.2.3. *Sound wave propagation in mean flow medium—two-dimensional case*

Simulation of the sound wave propagation in the medium with uniform mean flow is presented here. Figure 21 shows the case when a field is excited at the center with a single shot sine wave of the duration 40 Δt. The field model is shown in Figure 21(a) and the results are illustrated in (b). When the wave propagates down the stream, the wavelength is enlarged, while it shortens for the wave against the stream. Figure 22 shows the case of the partial mean flow. The sound is excited at a point in the flow region. The initial propagation is similar to the case of Figure 21, until the wave reaches the boundary between the flow and still regions at which it is partially reflected. The concentric propagation is recovered in the still region. Figure 23 shows the case when a line source is placed parallel to the direction of the flow. The propagation direction is tilted toward the direction of the downstream. The results thus simulated all look reasonable.

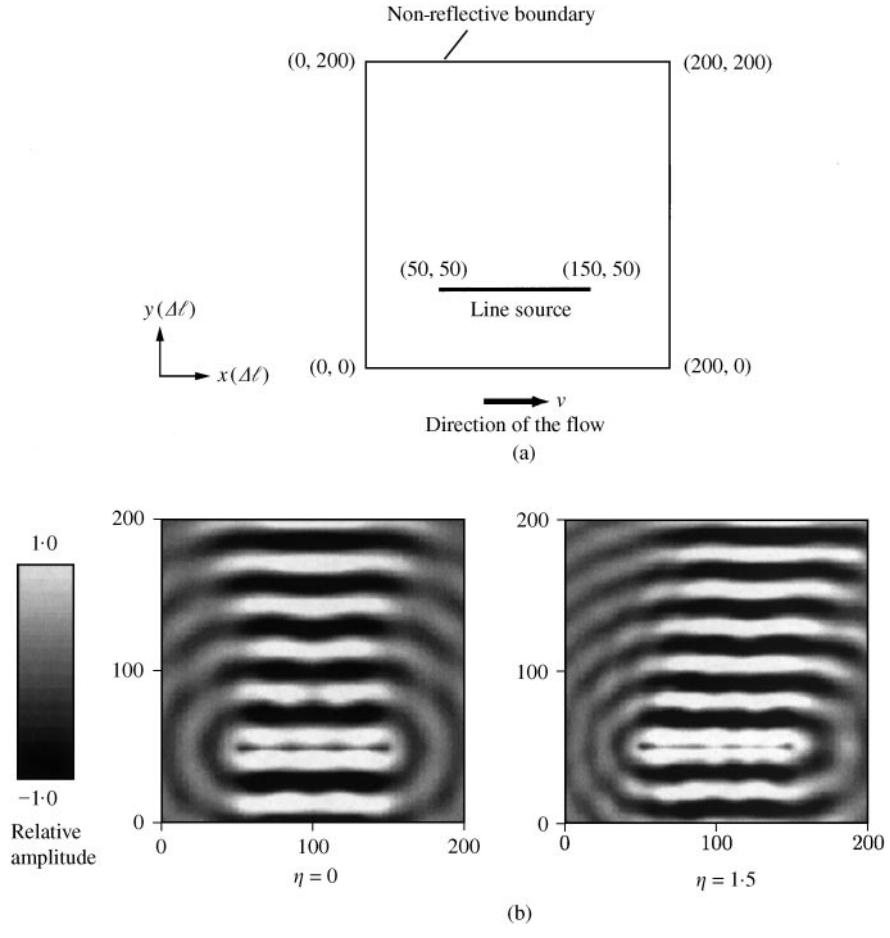

Figure 23. Sound propagation from a line sound source, $\eta = 1{\cdot}5$; (a) field model; (b) distributions.

4. CONCLUDING REMARKS

We presented the elements for modelling the sound wave in variable propagation velocity environment. The model for the case with mean flow was proposed in which the scattering algorithms were also presented. It was also shown that the modelling led to the wave equation that governed the wave propagation in the medium with mean flow. Some simple examples were demonstrated to verify the modelling and their solutions. The present modelling paves the way to the simulation of some problems, namely the automobile silencer problem, SODAR problem and ultrasonic flow-meter problem.

ACKNOWLEDGMENTS

The paper was partly presented at the 16th IMACS 2000 World Congress, Lausanne. R. Uehara and T. Masuda are acknowledged for their cooperation and help during the course of the present study.

REFERENCES

1. P. B. JOHNS and R. L. BEURLE 1971 *Proceedings of the IEE* **118**, 1203–1208. Numerical solution of 2-dimensional scattering problems using transmission-line matrix.
2. Y. YOSHII, T. YAMABUCHI and Y. KAGAWA 1976 *Spring Meeting Proceedings of the Acoustical Society of Japan*, 421–422. Application of transmission-line matrix (TLM) method to acoustical problems.
3. Y. KAGAWA, T. TSUCHIYA, B. FUJII and K. FUJIOKA 1998 *Journal of Sound and Vibration* **218**, 419–444. Discrete Huygens' model approach to sound wave propagation.
4. Y. KAGAWA, T. TSUCHIYA, K. FUJIOKA and M. TAKEUCHI 1999 *Journal of Sound and Vibration* **225**, 61–78. Discrete Huygens' model approach to sound wave propagation—reverberation in a room, sound source identification and tomography in time reversal.
5. M. L. MUNJAL 1987 *Acoustics of Ducts and Mufflers*. New York: Wiley-Interscience.
6. The marine acoustics society of Japan 1984 *Marine Acoustics, Fundamentals and Applications*. Tokyo: The Marine Acoustics Society of Japan.
7. K. V. MACKENZIE 1981 *Journal of the Acoustics Society of America* **70**, 807–812. Nine-term equation for sound speed in the ocean.